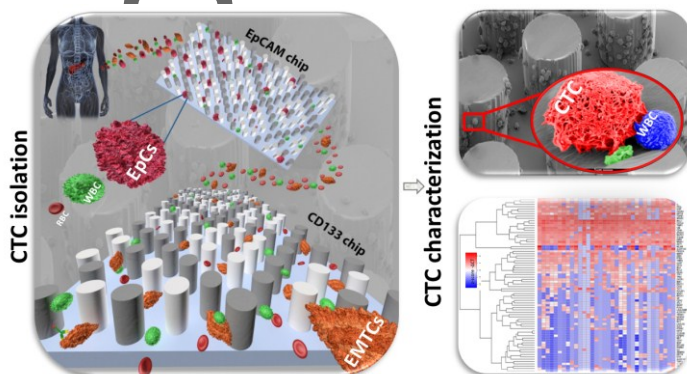# Table of content

The "Carpet Chip" technology uses sequential immunoaffinity-based microfluidic capture to study the biological relevance of heterogeneous CTC populations. Both epithelial CTCs (EpCs) and EMT-like CTCs (EMTCs) are detectable from the blood of pancreatic cancer patients. Based on our observations on EMTCs and patient lymph node involvement, targeting genes involved in the EMT process and individualizing therapies could reduce metastasis, thereby improving patient survival.

Profiling heterogeneous circulating tumor cells (CTC) populations in pancreatic cancer using a serial microfluidic CTC Carpet Chip

Mina Zeinali, Vasudha Murlidhar, Shamileh Fouladdel, Shimeng Shao, Lili Zhao, Heather Cameron, Armand Bankhead III, Jiaqi Shi, Kyle C.Cuneo, Vaibhav Sahai, Ebrahim Azizi, Max S. Wicha, Mathias Hafner, Diane M. Simeone,* Sunitha Nagrath*

*Co-corresponding authors

Mina Zeinali, Vasudha Murlidhar, Shimeng Shao, and Sunitha Nagrath: Department of Chemical Engineering and Biointerfaces Institute, University of Michigan, 2800 Plymouth Road, NCRC B10-A184, Ann Arbor, MI 48109, snagrath@umich.edu , 734- 647-7985

Mina Zeinali, Vasudha Murlidhar, Shamileh Fouladdel, Shimeng Shao, Ebrahim Azizi, Max S. Wicha and Sunitha Nagrath: Biointerfaces Institute, University of Michigan, 2800 Plymouth Road, NCRC, Ann Arbor, MI, USA 48109

Mina Zeinali and Prof. Mathias Hafner: Institute for Medical Technology of Heidelberg University & University of Applied Sciences Mannheim, Mannheim, Germany, 68163

Shamileh Fouladdel, Vaibhav Sahai, Ebrahim Azizi, Max S. Wicha:Department of Internal Medicine, University of Michigan, Ann Arbor, MI, USA 48109

Lili Zhao and Armand Bankhead III: Biostatistics Department, University of Michigan, Ann Arbor, MI, USA 48109

Armand Bankhead III: Department of Computational Medicine and Bioinformatics, University of Michigan, Ann Arbor, MI, USA 48109

Jiaqi Shi: Department of Pathology, University of Michigan, Ann Arbor, MI, USA 48109

Kyle C.Cuneo: Department of Radiation Oncology, University of Michigan, Ann Arbor, MI, USA 48109

Heather Cameron and Dr. Diane M. Simeone: Department of Surgery and Molecular and Integrative Physiology, 1500 E. Medical Center Drive, 2210B Taubman Center, Ann Arbor, MI 48109, simeone@med.umich.edu , 734-615-1600

Abstract

Although isolation of circulating tumor cells (CTCs) from pancreatic adenocarcinoma patients is feasible, investigating their clinical utility has proven less successful than other cancers due to limitations of EpCAM-only based CTC assays. We present an integrated technology and biology-based approach using a microfluidic "Carpet Chip" to study the biological relevance of heterogeneous CTC populations. We isolated both epithelial CTCs (EpCs) and EMT-like CTCs (EMTCs) simultaneously from whole blood of pancreatic cancer (PaCa) patients (n=35) by separately targeting two surface markers: EpCAM and CD133. Recovery of cancer cell lines spiked into whole blood was ≥97% with >76% purity. 34 patients (97.1%) had ≥5 EpCs per mL and 35 patients (100%) had ≥15 EMTCs per mL. Overall, we recovered significantly higher numbers of EMTCs than EpCs, reflecting the aggressive nature of pancreatic cancer. Furthermore, higher numbers of EMTCs were

observed in patients with lymph node involvement (N1) compared to patients without. Gene expression profiling of CTCs from 17 patients revealed that CXCR1 was significantly upregulated in EpCs, while known stem cell markers POU5F1/Oct-4 and MYC were upregulated in EMTCs. In conclusion, we demonstrated successful isolation and genomic profiling of heterogeneous CTC populations (EpCs and EMTCs), revealing genetic signatures relevant to patient outcomes.

1   Introduction

Pancreatic adenocarcinoma (PDAC) is the fourth leading cause of cancer-related death in the United States.[1] The median survival time is less than 6 months, with a bleak 5-year survival rate of 8 percent, making it one of the most lethal malignancies in humans.[1] Lack of early symptoms and reliable screening tests for early detection are major reasons why over 85% of PDAC patients are inoperable at the time of diagnosis.[2]

Since access to tumor biopsies in pancreatic cancer (PaCa) is quite challenging due to its anatomical positions, biomarkers are required to provide better diagnosis and explore alternative therapies. One avenue that holds promise in developing accurate predictive tools and pharmacodynamic biomarkers to guide patient care is the analysis of circulating tumor cells (CTCs).[3-9] Detection, quantification, and molecular characterization of CTCs in peripheral blood have been recognized as highly valuable emerging techniques in the diagnosis of cancer and detection of metastasis.[3, 7, 10, 11] CTCs are cells that extravasate from the primary tumor, enter the blood stream, enabling their transportation to distant sites and potential formation of metastatic tumors.[2, 3, 12] CTCs may enter the blood circulation in two ways: by passive shedding of tumor cells from the primary tumor, which may occur in large numbers and in early stages of tumor formation, or by an active mechanism involving the epithelial-to-mesenchymal transition (EMT).[2] EMT is a complex molecular and cellular

program by which cells of epithelial origin lose their apical-basal polarity and adhesiveness to neighboring cells and gain mesenchymal features including aggressiveness, motility, invasiveness, and resistance to apoptosis.[2, 5] Thus, EMT can be molecularly defined by tumor cells losing intracellular adhesions, with down-regulation of epithelial markers (e.g. epithelial cell adhesion molecule (EpCAM) and cytokeratins) and up-regulation of mesenchymal markers (e.g. CD133, vimentin).[13]

Cancer stem cells (CSCs) and cells undergoing EMT play important roles in tumorigenesis, metastasis, and chemo and radio-resistance.[14, 15] Therefore, detecting and analyzing these cells among CTCs in circulation could lead to better understanding of EMT, and tumor metastasis. CD133 expressed on the cell surface is now recognized as a prospective marker for the isolation and characterization of pancreatic stem and progenitor cells.[16-18] CD133+ pancreatic CSCs showed more aggressive behavior such as increased cell proliferation, migration, and invasion compared with the CD133- cells because they underwent EMT more readily.[19-21]

Detection and isolation of CTCs is challenging due to the low number of CTCs in the blood (on the order of 1 CTC per 10^6–10^9 normal blood cells) and the biological heterogeneity of CTCs.[22] Multiple approaches have been considered to overcome the limitation of low numbers of CTCs in peripheral blood, including immunoaffinity based methods, size-based separation, Ficoll density gradient, dielectrophoresis, negative depletion, and inertial methods.[23] Microfluidic isolation techniques have become attractive since the development of the first microfluidic CTC Chip [4] due to their high sensitivity, high throughput, low cost, and enhanced spatio-temporal control abilities.[4, 9] However, although antibody-based capture methods offer high specificity, most reported technologies lack the ability to capture biologically heterogeneous populations of CTCs. The main approach for enrichment thus far has been to capture cells of interest by using specific epithelial markers

such as EpCAM on the cell surface to distinguish CTCs from leukocytes.[3] However, EpCAM-based approaches could potentially miss a substantial portion of CTCs that have lost expression of epithelial markers and have undergone the process of EMT.[11, 24]

Herein, we present an integrated technology and biology-based translational approach using two CTC Carpet Chips in sequence to identify and study the biological relevance of rare heterogeneous population of circulating cells, including both epithelial CTCs (EpCs) and EMT-like CTCs (EMTCs), simultaneously from the peripheral blood of PaCa patients (Figure 1). We have focused on a novel strategy based on obtaining separate populations of phenotypically distinct CTCs.

Obtaining pure CTC populations is crucial for a robust downstream gene analysis. Herein, by applying the novel sequential microfluidic Carpet CTC Chip with different spacing between posts and arrays, we demonstrated enumeration, detection, and downstream mRNA genetic analysis of distinct CTC populations (EpCs and EMTCs) from PaCa patients. We profiled the mRNA expression of both of these populations using a panel of 96 cancer-related genes (Table S1).

In the current work, for a more thorough representation of biologically diverse CTCs in patients with pancreatic cancer sequential microfluidic devices were set up using antibodies against EpCAM, to capture EpCAM+ CTCs, and antibodies against CD133 to capture more stem cell like cells, or putative EpCAM- CTCs.[25]

2 Results and Discussion

2.1 CTC Carpet microfluidic Chip technology

The CTC Carpet Chip is designed to capture heterogeneous populations of rare CTCs using antibody-coated microposts.[4] In order to increase the sensitivity of capture phenotypically distinct CTCs, the previous CTC-Chip design developed by Nagrath et al. was

modified by implementing an 18° rotation of hexagonal arrays of 100 μm x 100 μm microposts with an average distance of 50 μm between them (Figure S3A). We have incorporated novel rearrangements of the posts which greatly enhances the capture of EpCs on one chip, while reducing off-target capture, including EMTCs. This employs a dual immunoaffinity and physical discrimination approach enabled by the lateral flow distribution and cell post interactions within the CTC Carpet Chip. The CTC Carpet Chip has around 80,000 microposts and the overall size of the microfluidic device is 44.6 mm × 16.9 mm. The design of the CTC Carpet Chip and representative SEM images of the microposts are shown (Figure 2A).

Successful capture of each population with high specificity and sensitivity was dependent on the flow velocities and shear forces within the device. The flow velocity was optimized to allow maximal contact between cells and microposts, while shear forces were sufficient to prevent non-specific cell attachment to posts. Different micropost geometries and arrangements of the arrays and other parameters were explored in the process of optimization of the CTC Carpet Chip (Figure S2 and S3). The aspect ratio, spacing, angle, micropost distribution, along with streamlines were optimized to increase capture efficiency for target cells while maintaining minimal non-specific binding. The velocity magnitude profile and particle tracing plot on a portion of the diamond shape of the CTC Carpet Chip are shown in Figure 2B-C. Cell trajectories (blue lines) are based on particle tracing and the end position of the cells is shown by red dots (Figure 2C). The simulations clearly had shown the lateral distribution of fluid around the Carpet design as well as effective cell post interactions. The CTC Carpet Chip was fabricated using standard photolithography techniques to create a silicon mold, followed by PDMS replica molding, and functionalized as previously described (Figure S1).[26]

2.2 Single/dual CTC Carpet Chip optimization

Four cancer cell lines with different levels of EpCAM expression and one cell line with high CD133 expression were used for testing and optimization of the CTC Carpet Chip: colon cancer line HT-29 and pancreatic cancer line Panc-1 (high EpCAM expression), prostate cancer line PC-3 (low EpCAM expression), breast cancer line Hs-578T (no EpCAM expression/negative control) and pancreatic cancer line Capan-1 (high CD133 expression).[27] These cell lines were labeled with green CellTracker dye (GCT) (described in the supplementary) and spiked into blood at a concentration of 1000 cells mL^{-1} to test the capture efficiencies of the single CTC Carpet Chip functionalized with either anti-EpCAM or anti-CD133 antibodies. The CTC Carpet Chip yielded the following efficiencies across the different cell lines; 97.5%±2.2 (HT-29) and 94.9%±2.4 (Panc-1), 87.7%±13.9 (PC-3), 13.6% (Hs-578T), and 73% ±16.6 (Capan-1) (Figure 3A). Thus, high capture efficiencies were observed using different cell lines using single CTC Carpet chip.

To capture different subpopulations of CTCs (EpCs and EMTCs) simultaneously from the same blood, we connected two devices functionalized with different antibodies (anti-EpCAM in one device and anti-CD133 in the other device) in series as shown in Figure 3B. Therefore, distinct populations could be easily identified and separately made available for downstream gene analysis. Blood was passed through the connected chips at a flow rate of 1mL hr^{-1} through the inlet of the first device. Four different set-ups were tested in order to evaluate the sensitivity and specificity of the capture rates of the chips, each coated with and without the antibodies of interest (anti-EpCAM and anti-CD133), using Panc-1 spiked into blood. Chips coated with no antibodies (EpCAM- and CD133-) showed <3% capture efficiency (false positive). However, in the presence of antibodies (EpCAM+ and CD133+), efficiency rates increased to 89.8%±9.5 EpCAM$^+$ cells and 6.6%±3.3 CD133+ cells. EpCAM+ and CD133- dual chips showed 90.2% and 0.7% EpCAM+ and CD133+ cells capture efficiencies. EpCAM- and CD133+ dual chips captured 2.4% and 7.2% EpCAM+

and CD133+ cells capture efficiencies (Figure 3C), demonstrating high specificity and consistent yields for both of the captured antibodies in the dual isolation. In summary, applying dual CTC Carpet chip technology in terms of isolating different type of cancer cells was quite sensitive and specific.

A pseudo-colored SEM image of captured cancer cells spiked into blood on the CTC Carpet Chip is shown in Figure 3D. After capture, cancer cells were detected by immunofluorescence staining protocol described in Methods. Pan-CK$^+$/CD45$^-$/DAPI$^+$, and Vim$^+$/CD45$^-$/DAPI$^+$ phenotypes were determined and enumerated as EpCs and EMTCs respectively. Figure 3E shows confocal images of captured cancer cells stained for Pan-CK (red) and CD45 (green) to distinguish EpCs and WBCs. The captured EMTCs in the CD133 chip are shown in Figure 4C, with Vim (orange) and CD45 (green) used as detection antibodies for the EMTCs and WBCs respectively.

2.3   Application of technology to evaluate heterogeneity in clinical samples

We used the microfluidic chip to analyze fresh blood samples from PaCa patients. Thirty-five patients with histologically documented PDAC of varying stages were analyzed, with clinical data provided in Table S2. Blood samples from nine healthy controls (HC) were used for comparison.

The dual CTC Carpet Chips were connected in the sequential order of EpCAM first followed by CD133 in order to capture the EpCs and EMTCs (Figure S4) and then whole blood collected from the patients was flowed through the chips at 1mL hr^{-1} (Figure 3B). However, to increase the throughput in the future, one can apply a pre-depletion step like RBC removal using inertial separation utilizing spiral devices.[28]

Figure 4A-B show representative images of EpCs cells (Figure 4A) on the EpCAM chip captured from PaCa patients. EpCs demonstrating varied morphologies, ranging from round to oval in shape and in some cases occurring as cluster (Figure 4B). Figure 4C shows

images of an EMTC and a leukocyte. As shown in Figure 4D, EMTCs captured on the chip had a wide range of cell sizes. Red, orange, and green arrows indicate Pan-CK, Vim, and CD45 staining respectively. Figure 4E shows a representative confocal image of a EMTC (pink) and a WBC (green) captured from a PaCa patient on the CD133 chip. To determine the presence of EpCs+ in the CD133 chip and EMTCs+ in the EpCAM chip, 16 patient samples were tested through triple staining of each chip (Pan-CK and Vim along with CD45) (Figure S5). A small number of double positive (Pan-CK$^+$/CD45$^+$) cells were found in some samples and were excluded from this study due to unknown origin and significance.

We quantified the captured EpCs and EMTCs on EpCAM and CD133 chips and found that 97.5% of the patients had EpCs+ ($\geq$5 Pan-CK+ CTCs per mL) with a mean of 22.4±17.7 per mL, while all 35 patients had EMTCs ($\geq$15 Vim+ CTCs per mL) with a mean of 85.7±59.5 per mL. In contrast, low numbers of EpCs (0.9±0.9 per mL) and EMTCs (1.9±2 per mL) were observed in the HCs (Figure 5A). In summary, the results indicate significant differences between the overall number of CTCs in PaCa patients samples (108.1±63.5) vs. HCs (2.8±2.6) (p<0.0001), as well as the number of EpCs (20.8% of overall CTCs) vs. EMTCs (79.2% of overall CTCs). We found significantly higher numbers of EMT-like CTCs in circulation in PaCa patients compared to epithelial CTCs (p<0.0001).

2.4 CTCs enrichment by using the CTC Carpet Chip to explore associations with clinical outcomes

To further explore the relationship of EpCs and EMTCs and clinical outcomes in the PaCa patient cohort (n=35), the CTC counts from these two cell populations were analyzed based on clinical disease stages (Figure 5B-G). All stages except stage IIA showed significantly higher numbers of EMTCs compared to the number of EpCs (Figure 5B). Patients with stage IV disease showed higher numbers of EMTCs than EpCs (p=0.0008), suggesting the strong role of the EMT process in the metastatic progression of pancreatic cancer.[2, 5, 10, 29-31]

Also, patients were categorized based on the tumor status as resectable (n=9), borderline resectable (n=2), locally advanced (n=13), and metastatic (n=11) groups. There were significantly higher numbers of EMTCs than EpCs between all these groups, except borderline resectable patients due to the small sample numbers (Figure 5C). The ratio of EpCs/EMTCs to total number of CTCs has a decreasing/increasing trend with later stages (Figure 5D). The percentage of EpCs decreased toward late stages, whereas the percentage of EMTCs increased. Figure 5E-G summarize the frequencies of EpCs and EMTCs characterized in different patient subgroups, including tumor size <2cm vs. >2cm, no lymph node involvement (N0) vs. lymph node involvement (N1), and non-metastatic (M0) vs. metastatic (M1) groups. Significantly higher numbers of EMTCs (p=0.04) were observed when the patients were grouped based on lymph node involvement (N1) compared with no lymph node involvement (N0) patients. This supports the observations from other studies, where the associations of EMT with lymph node metastasis have been reported.[32-34] However, we were not able to observe any significant correlation between CTC abundance, tumor size, metastatic burden, operability, and survival rate in this cohort which could be due to the limited sample size.

2.5   Gene expression profiling of EpCs and EMTCs by qRT-PCR

RNA was extracted from captured CTCs and utilized for gene expression profiling by RT-qPCR. The gene expression profiles of CTCs isolated from blood samples of PaCa patients (n=17) which were run through the dual CTC Carpet Chip are shown in Figure 6. Figure 6A presents the heat map of expression levels of genes. Figure 6B presents the median log fold change of select genes with logFC>1.5. Among these genes, ERCC1 showed >1.5 logFC in the CTCs captured on EpCAM coated chip which is correlated with significantly better overall survival (OS) and progression free survival (PFS). The histological staining and

immunohistochemistry (IHC) analysis of some of these markers in the primary PDAC tissues are shown in Figure S6.

Figure 6C-D presents box plots showing expression of significant differential expression of genes in patient CTCs isolated by EpCAM and CD133 chips. CXCR1 (p=0.03) in the EpCAM chip (Figure 6C), and POU5F1 (or Oct-4) (p=0.008) and MYC (p=0.03) in CD133 chip (Figure 6D) were significantly differentially expressed. Given the phenotypic differences we have observed between EpCs and EMTCs, it is not surprising that the stem cell related gene POU5F1 (OCT4) is highly expressed in EMTCs. Based on our results, over expression of this gene was significantly correlated with worse PFS.

Signaling pathways based on analysis of captured CTCs on EpCAM chip compared to CTCs on CD133 chip with iPathwayGuide suggested that these two genes (POU5F1 and MYC) were involved in signaling pathways regulating pluripotency of stem cells.

To further explore the gene signatures in different stages of disease, the patients were grouped based on their disease stages (Figure 7). The summary of selected genes (p<0.05) are shown in the box plots. Stage IIA patients showed significant differential expression of genes including ATL1, BMi1, CD14, CDH2, ERCC1, MKi67, TTF1, and Vim compared to all other stages (Figure 7A-i). We also compared protein level expression of select differentially expressed markers by immunohistochemistry of primary tissues. The hematoxylin & eosin (H&E) staining of the primary PDAC tissues of early stage patients is shown in Figure 7A-ii. The corresponding primary tumor tissues were highly positive (intensity of 3, 100% positivity) for BMi1 protein expression and moderate positive (intensity of 2, 10% positivity) for MKi67 protein expression shown by immunohistochemistry (IHC) analysis (Figure 7A-iii).

PaCa patients in stages IIB&III showed significant differential expression of ALDH1A3, ESR1, KRT18 and KRT19 compared to stage IIA (Figure 7B-i). Comparing

stages IIB&III with stage IV patients reveled significant differential expression of genes including AKT1 and CD3D (Figure 7B-ii). Stage IV patients showed significantly elevated expression of CDH1, DCN, KRT19, PGR, and PIK3CA genes compared to the rest of the stages (Figure 7C-i). The H&E staining of the primary PDAC tissue of late stage PaCa patients is shown in Figure 7C-ii. The protein expression of PIK3CA in the corresponding primary tumor tissues was moderate (intensity of 2, 20% positivity) (Figure 7C-iii).

2.6 Molecular signature and prognosis

In the cohort considered in this study, the median OS of all patients was 15±10.2 months (2.5-33.7) and the median PFS was 5.6±10.5 months (1.7-33.5). The survival estimated by Kaplan Meier (KM) were significantly better for patients with high expression of AKT1 (21.1 vs. 6 months p=0.08 for OS, and 11.6 vs. 4.6 months p=0.03 for PFS), BMi1 (20.4 vs. 13.6 months p=0.04 for OS, and 9.2 vs. 4.6 months for PFS), CDH2 (30.2 vs. 14.8 months p=0.04 for OS, and 6.9 vs. 5.1 months for PFS), ERCC1 (22.3 vs. 10.6 months p=0.04 for OS, and 11.7 vs. 4.6 months p=0.02 for PFS), IL8 (21.1 vs. 6 months p=0.08 for OS, and 11.6 vs. 4.6 months p=0.03 for PFS), TTF1 (20.4 vs. 12.8 months p=0.08 for OS, and 9.3 vs. 2.5 months p=0.04 for PFS), and TP53 (18 vs. 11.4 months for OS, and 10 vs. 4.6 months p=0.03 for PFS) (Figure 8A-G). The H&E staining of the primary PDAC tissue of a PaCa patient is shown in Figure 8H-i. IHC analysis of TP53 protein expression in the corresponding primary tumor tissue showed high positivity (intensity of 2, 90% positivity) of this marker (Figure 8H-ii). PaCa patients with higher expression of metastatic marker GEMIN2 (5 vs. 18 months p=0.01[*] for OS, and 4.6 vs. 7.7 months for PFS), and stem marker POU5F1 (13.4 vs. 20.4 months for OS, and 4.6 vs. 10.1 months p=0.04[*] for PFS) showed worse OS or PFS respectively (Figure 8I-J).

Among these analyzed genes, as mentioned before, BMi1, CDH2, ERCC1 and TTF1 which showed higher expression in early stage patients (stage IIA) compared to the rest of

stages which were also significantly associated with prolonged OS and/or PFS. However, PaCa patients with higher expression of stem marker POU5F1 showed worse PFS. Overall, isolating different CTC populations separately may help us predict the patient's outcome.

3 Conclusion

CTC detection based only on EpCAM might miss a substantial number of other CTCs, which might have an aggressive phenotype such as EMTCs.[11, 35] We were able to detect distinct heterogeneous CTC population (EpCs and EMTCs) simultaneously from PaCa patient samples by utilizing the novel sequential microfluidic Carpet CTC Chip. Different spacing between posts and arrays, enabled us to increase the capture efficiencies (>97%) and purity (>76%), which is crucial for downstream gene analysis.

Recent advances have enabled the detection of CTCs in various cancer types, however, the clinical utility of CTCs in pancreatic cancer needs to improve.[36] By detecting and analyzing primary tumor-derived circulating tumor cells, we would obtain useful information about disease status noninvasively. This data could provide valuable information to improve diagnosis and treatment of pancreatic cancer. There have been no prior reports correlating the EpCs and EMTCs circulation in PaCa.

Hence, we have developed sequential microfluidic CTC Carpet Chip using antibodies against EpCAM, to capture EpCAM+ CTCs, and antibodies against CD133 to capture more stem cell like cells, or putative EpCAM- CTCs in simultaneously from the peripheral blood of PaCa patients.[25] Although, the current study are performed with sequential devices, once can combine both the chips into a single device with a multilayer fabrication approach. Our results indicate that enumeration, detection, and molecular characterization of these CTC populations show a great promise as a diagnostic and therapeutic tool for detection of cancer and metastasis. Our findings on gene expression profiling of CTCs from early stage PaCa

patients may improve prediction of survival and outcomes. Finally, based on our observations on EMTCs and lymph node involvement, targeting the genes involved in the EMT process and individualized therapy could reduce metastasis, thereby increasing the survival rate of PaCa patients.[29]

4   Experimental Section

4.1   Computational analysis of the microposts:

Finite element simulations were performed in COMSOL Multiphysics 4.2 (Comsol Inc.) with an inlet flow rate of 1 mL hr^{-1} on a portion of diamond shape of the CTC Carpet Chip. A symmetry boundary condition was applied on the two similar boundaries flanking the posts. A wall (no slip) boundary condition was applied on the post outlines. The particle tracing plot was simulated with rigid particles 15 μm in size, with a condition of sticking to any encountered wall being applied.

4.2   Capture efficiency of single CTC Carpet Chip

Four different cancer cell lines with different EpCAM expression levels, colon cancer line HT-29, pancreatic cancer line Panc-1, prostate cancer line PC-3, and breast cancer line Hs-578T, and CD133 positive pancreatic cancer line Capan-1 were fluorescently-labeled with green CellTracker dye (GCT) (Invitrogen). To determine the percentage of cells captured on a functionalized CTC Carpet Chip, coated with either anti-EpCAM (for EpCAM expression cell lines) or anti-CD133 (for CD133 expression cell line), 1000 cells from each of the fluorescently-labeled cancer cell lines were spiked into whole blood collected from healthy controls (HCs) and flowed through the microfluidic device at a constant flow rate (1mL hr^{-1}). Then cells were fixed and permeabilized on the chip by using Cytofix/Cytoperm (BD Bioscience) followed by staining with DAPI (Invitrogen) to identify DNA content. Capture efficiency was calculated as the percentage of captured cells on the device divided by the

total number of cells flowed through the chip. Captured cancer cells were identified and enumerated by scanning the entire micropost chamber of the device using a Nikon Eclipse Ti fluorescence microscope.

4.3 Capture efficiency of dual CTC Carpet Chip

In order to facilitate separating circulating epithelial (EpCAM-expressing) and EMT-like (CD133-expressing) cells in different devices in sequential order from the same sample, two separate CTC Carpet Chips were connected to each other using a 2-inch piece of connective tubing (Fisherbrand™ Tygon S3™ E-3603 Flexible Tubings). The first chip was coated with anti-EpCAM and the second one with anti-CD133. The blood sample was then processed through each chip in succession. After this step, the chips were disconnected from one another, and washed with PBS (10 mL hr^{-1}) for the immunofluorescence staining process.

4.4 Patient CTC capture and immunofluorescence staining

This study was approved by the institutional review board (IRB) of the University of Michigan. 1mL of whole blood from each PaCa patient was processed through two CTC Carpet Chips connected in series at the designated flow rate (1mL hr^{-1}), followed by fixation and permeabilization with 4% paraformaldehyde (Pierce) and 0.2% Triton X-100 (Sigma) respectively, followed by blocking with 3% BSA (bovine serum albumin) (Sigma) plus 2% goat serum (Invitrogen).

In order to identify and characterize sub-populations of CTCs and distinguish them from other blood cells, we used the following criteria: cells that were captured on the anti-EpCAM coated chip and stained positive for pan-cytokeratin (Pan-CK) (AbDSerotec), negative for CD45 (AbDSerotec), and positive for cell nucleus staining (DAPI) (Invitrogen) were characterized as EpCs; and cells that were captured on the anti-CD133 coated chip and stained positive for Vimentin (Vim) (BD Bioscience), negative for CD45, and positive for

DAPI were characterized as EMTCs.[3] Alexa Fluor 488/546/647-conjugated secondary antibodies (Invitrogen) were applied in order to detect CD45, Pan-CK, and Vim respectively.

4.5 RNA extraction and qRT-PCR analysis

The mRNA extracted from CTCs were analyzed for gene expression for the selected panel of 96 cancer-related genes (Table S2). Isolated CTCs within the device were incubated at 42°C for 30 min with extraction buffer (Arcturus PicoPure kit, Invitrogen) to lyse the cells. Then RNase free water was passed through the chip to collect the cell lysate. Total RNA was then prepared from the CTC lysate using the Arcturus PicoPure kit (Invitrogen) and was subjected to a reverse transcription reaction followed by 18 cycles of pre-amplification of cDNAs of 96 genes of interest using the pooled TaqMan Gene Expression Assays and Cell-to-CT Kit (Ambion, Invitrogen). Finally, the gene expression pattern of pre-amplified cDNAs was determined using TaqMan Gene Expression Assays for 96 genes and the BioMark HD qPCR platform (35 cycles). Non-detect values were replaced by a pseudo cycle number of 40 and in the analyzed samples typically out of 96 genes, around 50% of them showed positive data. Also a cut off n>2 (greater than 2 patients displaying gene expression in each group for each gene) was applied when genes in different groups were compared to each other, and 75 of 96 genes met this criterion. GAPDH was used as an internal reference to normalize cycle threshold (Ct) values for the genes of interest by subtracting each gene expression value by GAPDH to generate a -ΔCt. Median fold changes were generated by dividing the median gene expression ($2^{-\Delta Ct}$) of group A by that of group B. Finally, statistical analysis of data was done on the -ΔCt values for each gene in the studied samples.

4.6 Immunohistochemistry (IHC)

A gastrointestinal pathologist reviewed each patient's hematoxylin & eosin (H&E) stained resection specimen and identified a representative section of formalin-fixed, paraffin-embedded tumor and normal tissue. The unstained 5μm -thick tissue section was reacted with

anti-BMi1 (Cell Signaling), anti-MKi67 (Cell Marque), anti-PIK3CA (Abcam), anti-P53 (Cell Marque), MCAM (Abcam), and CD133 (Miltenyi Biotec) antibodies using immunohistochemistry (IHC) technique to determine levels of tumoral protein expression of BMi1, MKi67, PIK3CA, TP53, MCAM, and CD133. The staining intensity and percentage of positive cells out of total tumor cells were graded by a pancreatic pathologist who was blinded to patients' outcomes. The intensity of IHC staining is graded on a scale of 0 to 3, where 0 is no staining, 1 is weak, 2 is moderate, and 3 is strong staining.

4.7 Statistical analysis

All results present as mean ± standard deviation. Unpaired t-tests (two-tailed) were used to compare the differences between total CTCs of patient samples (n=35) vs. healthy controls (n=9). Paired t-tests (two-tailed) were used to compare the differences between EpCs and EMTCs (n=35). Unpaired t-tests (two-tailed) were used to evaluate the effect of stage, resection, tumor size, lymph node involvement, and metastasis on EpCs and EMTCs levels (n=35). Statistical significance was defined as a two-sided p<0.05. The Wilcoxon signed-rank test was used in RNA expression for paired samples (n=17). The Mann-Whitney test was used to quantify differences in RNA expression for non-paired samples using the average -ΔCt value across both sample chips (n=17). Analyses were conducted using GraphPad Prism, Python, R software environment, and iPathwayGuide (Advaita). P-values were not adjusted for multiple testing due to the small number of patient samples. The median expressions of genes ($2^{-\Delta Ct}$) across all patients were used as cutoff points for the Kaplan Meier graphs. Log-rank (Mantel-Cox) tests were used to analyze the Kaplan-Meier overall survival (OS) and progression free survival (PFS) graphs in all patient CTCs samples (n=17). P-values threshold of 0.05 were used in the iPathwayGuide analysis.

5   References

1.   L., S. R.; D., M. K.; Ahmedin, J., *CA: A Cancer Journal for Clinicians* **2018,** *68* (1), 7-30. DOI doi:10.3322/caac.21442.

2.   Tjensvoll, K.; Nordgard, O.; Smaaland, R., *International Journal of Cancer* **2014,** *134* (1), 1-8. DOI Doi 10.1002/Ijc.28134.

3.   Alunni-Fabbroni, M.; Sandri, M. T., *Methods* **2010,** *50* (4), 289-97. DOI 10.1016/j.ymeth.2010.01.027.

4.   Nagrath, S.; Sequist, L. V.; Maheswaran, S.; Bell, D. W.; Irimia, D.; Ulkus, L.; Smith, M. R.; Kwak, E. L.; Digumarthy, S.; Muzikansky, A.; Ryan, P.; Balis, U. J.; Tompkins, R. G.; Haber, D. A.; Toner, M., *Nature* **2007,** *450* (7173), 1235-U10. DOI Doi 10.1038/Nature06385.

5.   Bednarz-Knoll, N.; Alix-Panabieres, C.; Pantel, K., *Cancer and Metastasis Reviews* **2012,** *31* (3-4), 673-687. DOI DOI 10.1007/s10555-012-9370-z.

6.   Kurihara, T.; Itoi, T.; Sofuni, A.; Itokawa, F.; Tsuchiya, T.; Tsuji, S.; Ishii, K.; Ikeuchi, N.; Tsuchida, A.; Kasuya, K.; Kawai, T.; Sakai, Y.; Moriyasu, F., *Journal of Hepato-Biliary-Pancreatic Surgery* **2008,** *15* (2), 189-195. DOI DOI 10.1007/s00534-007-1250-5.

7.   Kanwar, N.; Done, S., **2011.**

8.   Stott, S. L.; Hsu, C. H.; Tsukrov, D. I.; Yu, M.; Miyamoto, D. T.; Waltman, B. A.; Rothenberg, S. M.; Shah, A. M.; Smas, M. E.; Korir, G. K.; Floyd, F. P.; Gilman, A. J.; Lord, J. B.; Winokur, D.; Springer, S.; Irimia, D.; Nagrath, S.; Sequist, L. V.; Lee, R. J.; Isselbacher, K. J.; Maheswaran, S.; Haber, D. A.; Toner, M., *Proceedings of the National Academy of Sciences of the United States of America* **2010,** *107* (43), 18392-18397. DOI DOI 10.1073/pnas.1012539107.

9.   Zhang, Z.; Nagrath, S., *Biomed Microdevices* **29 January 2013**.

10.   Chen, C. L.; Mahalingam, D.; Osmulski, P.; Jadhav, R. R.; Wang, C. M.; Leach, R. J.; Chang, T. C.; Weitman, S. D.; Kumar, A. P.; Sun, L. Z.; Gaczynska, M. E.; Thompson, I. M.; Huang, T. H. M., *Prostate* **2013,** *73* (8), 813-826. DOI Doi 10.1002/Pros.22625.

11.   Pantel, K.; Alix-Panabieres, C., *Trends in Molecular Medicine* **2010,** *16* (9), 398-406. DOI DOI 10.1016/j.molmed.2010.07.001.

12.   Torphy, R. J.; Tignanelli, C. J.; Moffitt, R. A.; Soper, S. A.; Yeh, J. J., *Journal of the American College of Surgeons* **2013,** *217* (3), S30-S30.

13.   Satelli, A.; Li, S. L., *Cellular and Molecular Life Sciences* **2011,** *68* (18), 3033-3046. DOI DOI 10.1007/s00018-011-0735-1.

14.   Nel, I.; Jehn, U.; Gauler, T.; Hoffmann, A.-C., *Translational Lung Cancer Research* **2014,** *3* (2), 100-106. DOI 10.3978/j.issn.2218-6751.2014.03.05.

15.   Xu, L., *Frontiers in Bioscience-Landmark* **2013,** *18*, 795-802. DOI Doi 10.2741/4143.

16.   Hori, Y., *Adv Exp Med Biol* **2013,** *777*, 185-96. DOI 10.1007/978-1-4614-5894-4_12.

17.   Hatina, J., *Neoplasma* **2012,** *59* (6), 700-707. DOI Doi 10.4149/Neo_2012_092.

18.   Hatina, J.; Schulz, W. A.; Fischer, J.; Wahl, J.; Debatin, K. M.; Beltinger, C., *Deutsche Medizinische Wochenschrift* **2007,** *132* (31-32), 1629-1632. DOI DOI 10.1055/s-2007-984945.

19.   Moriyama, T.; Ohuchida, K.; Mizumoto, K.; Cui, L.; Ikenaga, N.; Sato, N.; Tanaka, M., *Cancer* **2010,** *116* (14), 3357-68. DOI 10.1002/cncr.25121.

20.   Zhang, Y.; Wei, J. S.; Wang, H.; Xue, X. F.; An, Y.; Tang, D.; Yuan, Z. X.; Wang, F. T.; Wu, J. L.; Zhang, J. J.; Miao, Y., *Oncology Reports* **2012,** *27* (5), 1599-1605. DOI Doi 10.3892/Or.2012.1681.

21.   Ding, Q.; Yoshimitsu, M.; Kuwahata, T.; Maeda, K.; Hayashi, T.; Obara, T.; Miyazaki, Y.; Matsubara, S.; Natsugoe, S.; Takao, S., *Human Cell* **2012,** *25* (1), 1-8. DOI DOI 10.1007/s13577-011-0037-9.

22.   Liberko, M.; Kolostova, K.; Bobek, V., *Crit Rev Oncol Hemat* **2013,** *88* (2), 338-356. DOI 10.1016/j.critrevonc.2013.05.002.

23.   Alix-Panabieres, C.; Pantel, K., *Nat Rev Cancer* **2014,** *14* (9), 623-631. DOI 10.1038/nrc3820.

24.   Tobias M Gorges; Ingeborg Tinhofer; Michael Drosch; Lars Röse; Thomas M Zollner; Krahn, T.; Ahsen, O. v., **2012**.

25.   Qiang Ding; Yumi Miyazaki; Koichiro Tsukasa; Shyuichiro Matsubara; Makoto Yoshimitsu; Takao, S., *Molecular Cancer* **2014**.

26.   Murlidhar, V.; Zeinali, M.; Grabauskiene, S.; Ghannad-Rezaie, M.; Wicha, M. S.; Simeone, D. M.; Ramnath, N.; Reddy, R. M.; Nagrath, S., *Small* **2014,** *10* (23), 4895-4904. DOI 10.1002/smll.201400719.

27.   Lee, H. J.; You, D. D.; Choi, D. W.; Choi, Y. S.; Kim, S. J.; Won, Y. S.; Moon, H. J., *Journal of the Korean Surgical Society* **2011,** *81* (4), 263-270. DOI 10.4174/jkss.2011.81.4.263.

28.   Chen, H., *Scientific Reports* **2018,** *8* (1), 4042. DOI 10.1038/s41598-018-22348-z.

29.   Beuran, M.; Negoi, I.; Paun, S.; Ion, A. D.; Bleotu, C.; Negoi, R. I.; Hostiuc, S., *Pancreatology* **2015**. DOI 10.1016/j.pan.2015.02.011.

30.   Fazlul H. Sarkar; Yiwei Li; Zhiwei Wang; Kong, D., **Oct. 2009**.

31.   Zhang, Z. Y.; Ge, H. Y., *Cancer Lett* **2013,** *336* (1), 34-45. DOI DOI 10.1016/j.canlet.2013.04.021.

32.   Yamada, S.; Fuchs, B. C.; Fujii, T.; Shimoyama, Y.; Sugimoto, H.; Nomoto, S.; Takeda, S.; Tanabe, K. K.; Kodera, Y.; Nakao, A., *Surgery* **2013,** *154* (5), 946-54. DOI 10.1016/j.surg.2013.05.004.

33.   Lahat, G.; Lubezky, N.; Loewenstein, S.; Nizri, E.; Gan, S.; Pasmanik-Chor, M.; Hayman, L.; Barazowsky, E.; Ben-Haim, M.; Klausner, J. M., *Annals of Surgical Oncology* **2014,** *21* (4), 750-757. DOI 10.1245/s10434-014-3946-5.

34.   Hiroshi, K.; Sonshin, T.; Kosei, M.; Yuko, M.; Taisaku, K.; Koki, M.; Qiang, D.; Masahiko, S.; Satoshi, I.; Sumiya, I.; Shinichi, U.; Hiroyuki, S.; Shoji, N., *Journal of Surgical Oncology* **2012,** *105* (7), 655-661. DOI doi:10.1002/jso.23020.

35.   Rhim, A. D.; Mirek, E. T.; Aiello, N. M.; Maitra, A.; Bailey, J. M.; McAllister, F.; Reichert, M.; Beatty, G. L.; Rustgi, A. K.; Vonderheide, R. H.; Leach, S. D.; Stanger, B. Z., *Cell* **2012,** *148* (1-2), 349-61. DOI 10.1016/j.cell.2011.11.025.

36.   Nagrath, S.; Jack, R. M.; Sahai, V.; Simeone, D. M., *Gastroenterology 151* (3), 412-426. DOI 10.1053/j.gastro.2016.05.052.

37.   Murlidhar, V.; Zeinali, M.; Grabauskiene, S.; Ghannad-Rezaie, M.; Wicha, M. S.; Simeone, D. M.; Ramnath, N.; Reddy, R. M.; Nagrath, S., *Small* **2014,** *10* (23), 4895-904. DOI 10.1002/smll.201400719.

38.   Campo, A. d.; Greiner, C., *Journal of Micromechanics and Microengineering* **2007,** *17* (6), R81-R95. DOI 10.1088/0960-1317/17/6/r01.
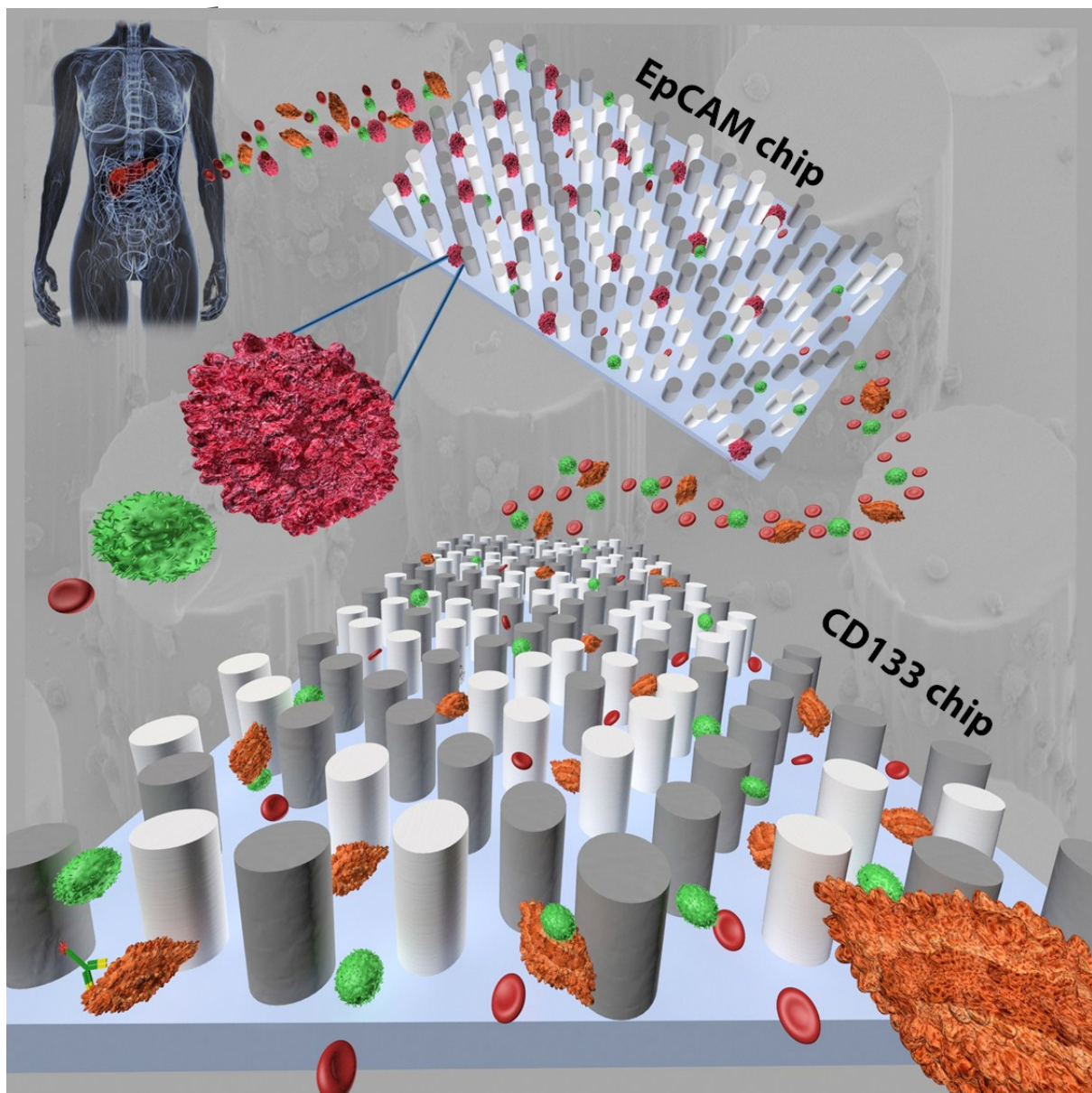
FIGURE LEGENDS

Figure 1: Dual capture strategy using CTC Carpet Chip. Schematic of the CTC Carpet Chips connected in series. Rare CTCs including both circulating epithelial cells (EpCs, dark pink) and EMT-like cells (EMTCs, orange) were captured simultaneously from the peripheral blood of pancreatic cancer (PaCa) patients by using two markers of interest, anti-EpCAM and anti-CD133, in two different chips. The white/red blood cells are shown in green/red respectively. The posts are displayed in different colors only for visualization of the device pattern. The video showing the capture principle and approach is available in the expanded view video (SV1).
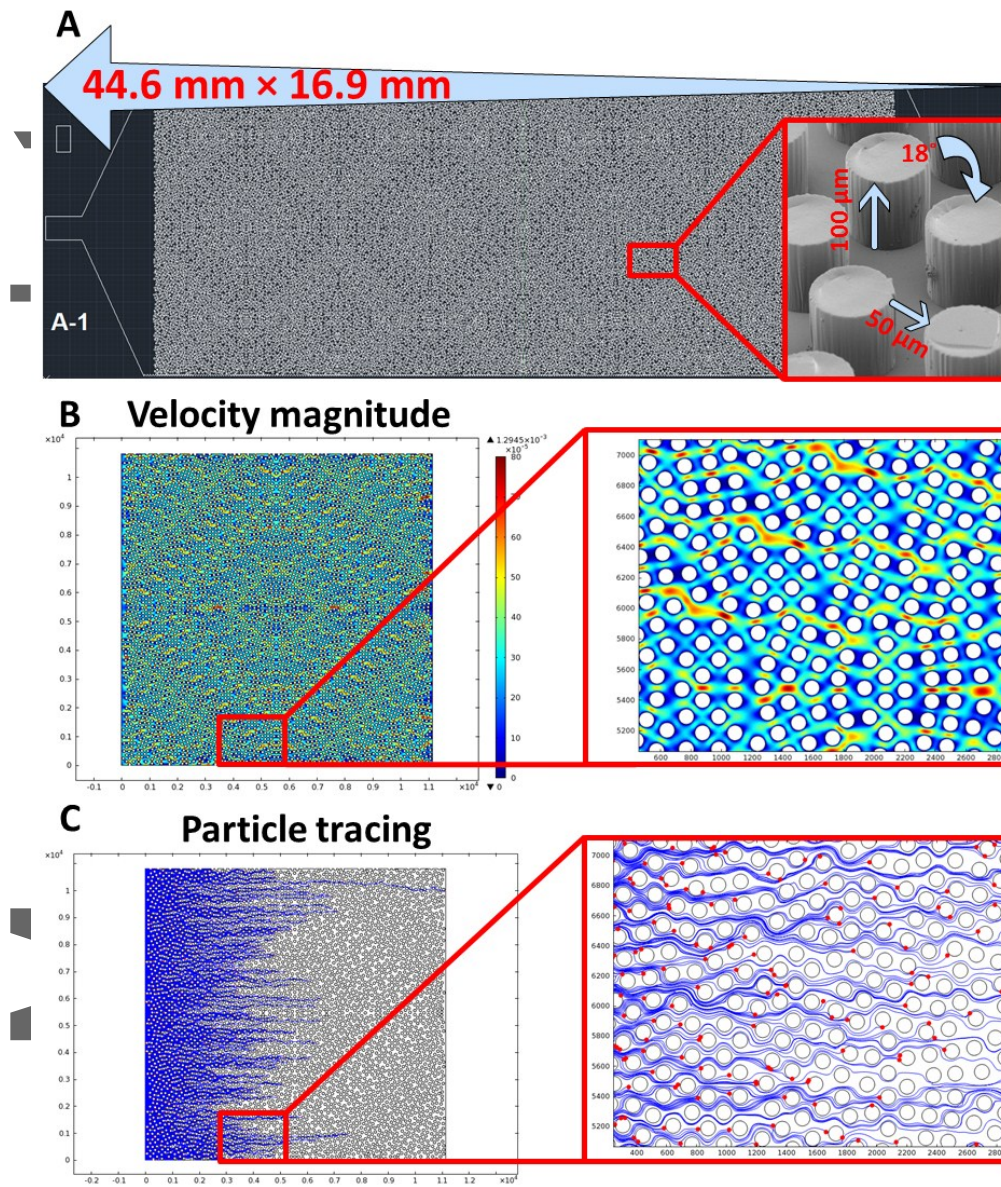
Figure 2: Schematic representation of CTC Carpet Chip and finite element simulations. A CTC Carpet Chip designed by AutoCAD software based on an 18° rotation of hexagonal arrays of 100 μm posts. It has around 80,000 post patterns with dimension of 100 μm × 100 μm, the distance between each post is 50 μm in which the posts are distributed in a way to have lateral flow. **B-C** Simulation studies were done by using COMSOL software to ensure the sensitivity and specificity of the designed chip. **B** Velocity magnitude of flow on a portion of diamond shape of the CTC Carpet Chip. **C** Particle tracing plot around microposts near the inlet demonstrating typical streamlines (blue) and capture of 15 μm rigid particles (red) upon encountering a wall (post).

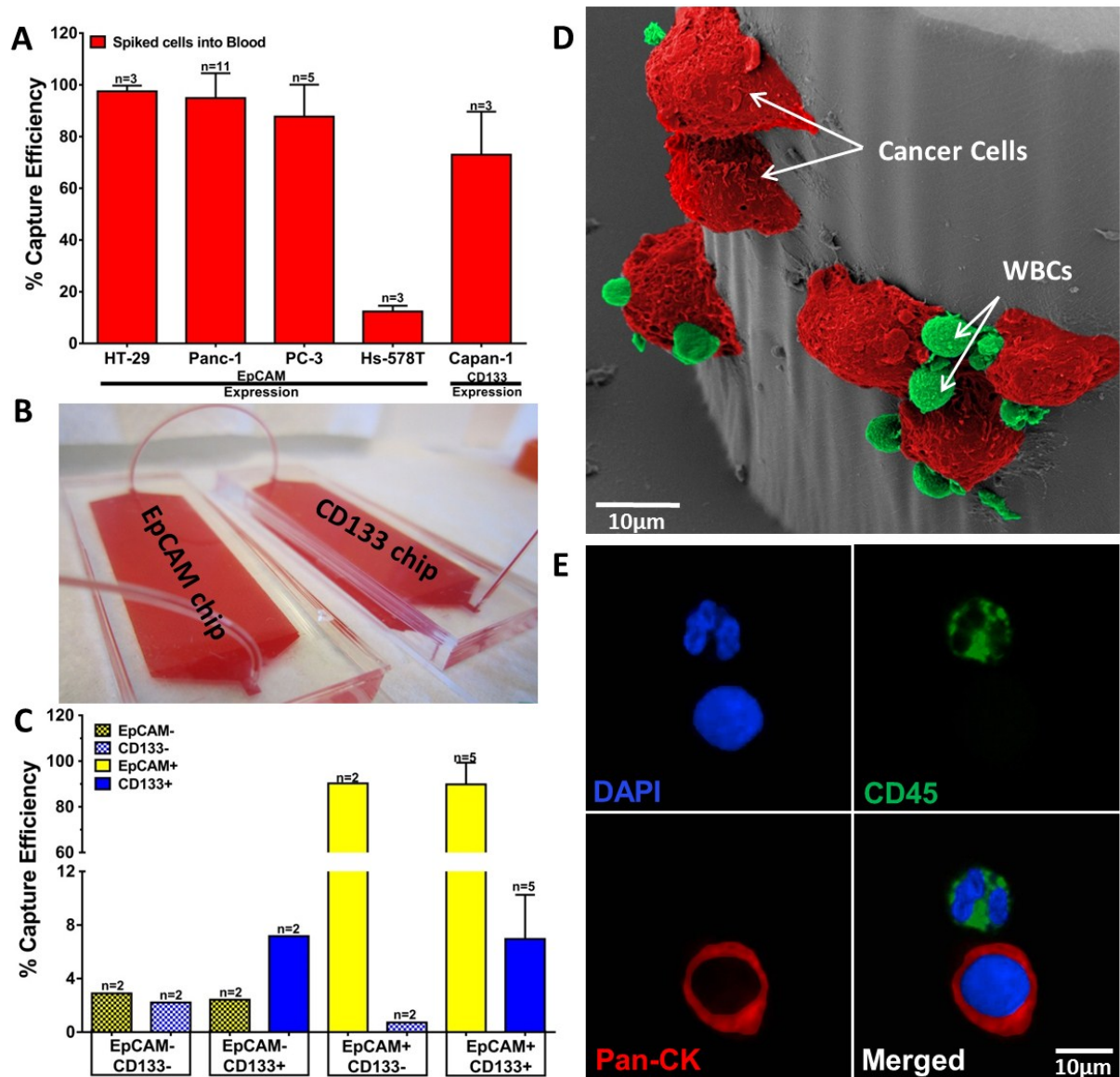**Figure 3: CTC Carpet Chip cell line optimization. A** Capture efficiency (%) of cell lines with various levels of EpCAM expression including HT-29 and Panc-1 (high EpCAM expression), PC-3 (low EpCAM expression), and Hs-578T (none), and one cell line with high CD133 expression (Capan-1). 1000 green CellTracker (GCT) cells were spiked into blood and processed through single CTC Carpet Chip coated with anti-EpCAM or anti-CD133. **B** Representative image showing dual CTC Carpet Chip; 1mL blood was sent through the anti-EpCAM coated CTC Carpet Chip which was connected to the anti-CD133 coated CTC Carpet Chip in sequence. **C** Capture efficiency (%) of Panc-1 cancer cells spiked into blood with or without antibodies (EpCAM and CD133) in the dual chips. The solid/hatched yellow and blue bars show the presence/absence of EpCAM and CD133 antibodies. **D** Pseudo-colored SEM image of the captured cancer cells spiked into blood on the CTC Carpet Chip. Cancer cells and WBCs are shown in red and green respectively. (E) Confocal image of a typical CK+ cancer cell is shown here. The Pan-CK+ CTCs were detected with Pan-CK (red) along with a CD45+ (green) WBC.
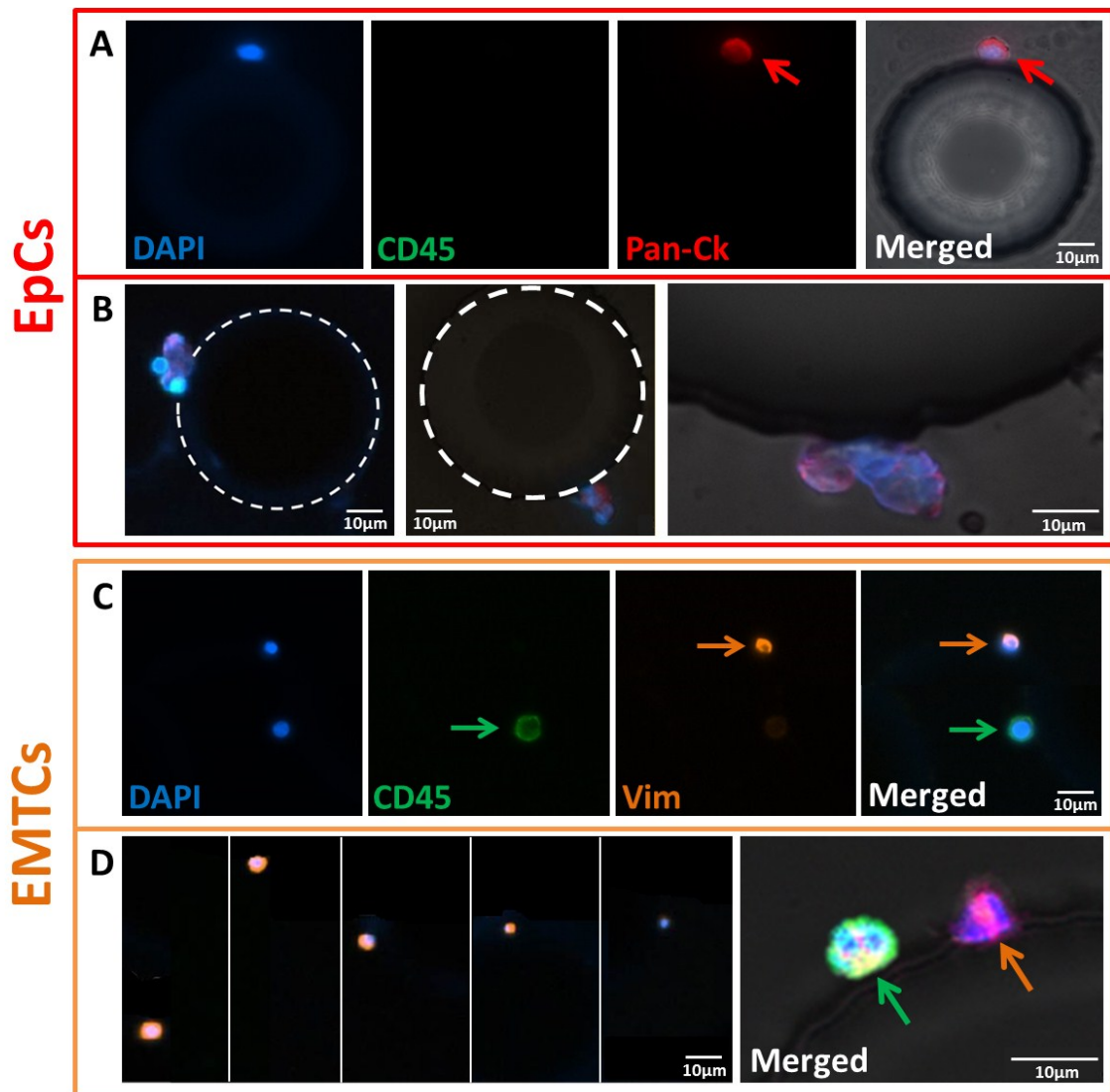
Figure 4: Characterization of circulating epithelial CTCs (EpCs) and EMT-like CTCs (EMTCs) in the EpCAM and CD133 Carpet Chip from PaCa patients. A EpCs and WBCs were stained with Pan-CK and CD45 respectively, in addition to DAPI. Red arrow is showing a Pan-CK EpC. **B** An EpC cluster captured around the posts. Post outlines are marked in white circle and bright field. The post outlines are marked with white circles. **C** Vimentin (orange) and CD45 (green) staining for detection of EMTCs and WBCs respectively. Orange and green arrows are showing Vimentin and CD45 positive cells respectively. **D** Different sizes of EMTCs captured on the device. **E** Confocal image of EMTC (pink) and WBC (green). All scale bars are 10μm.
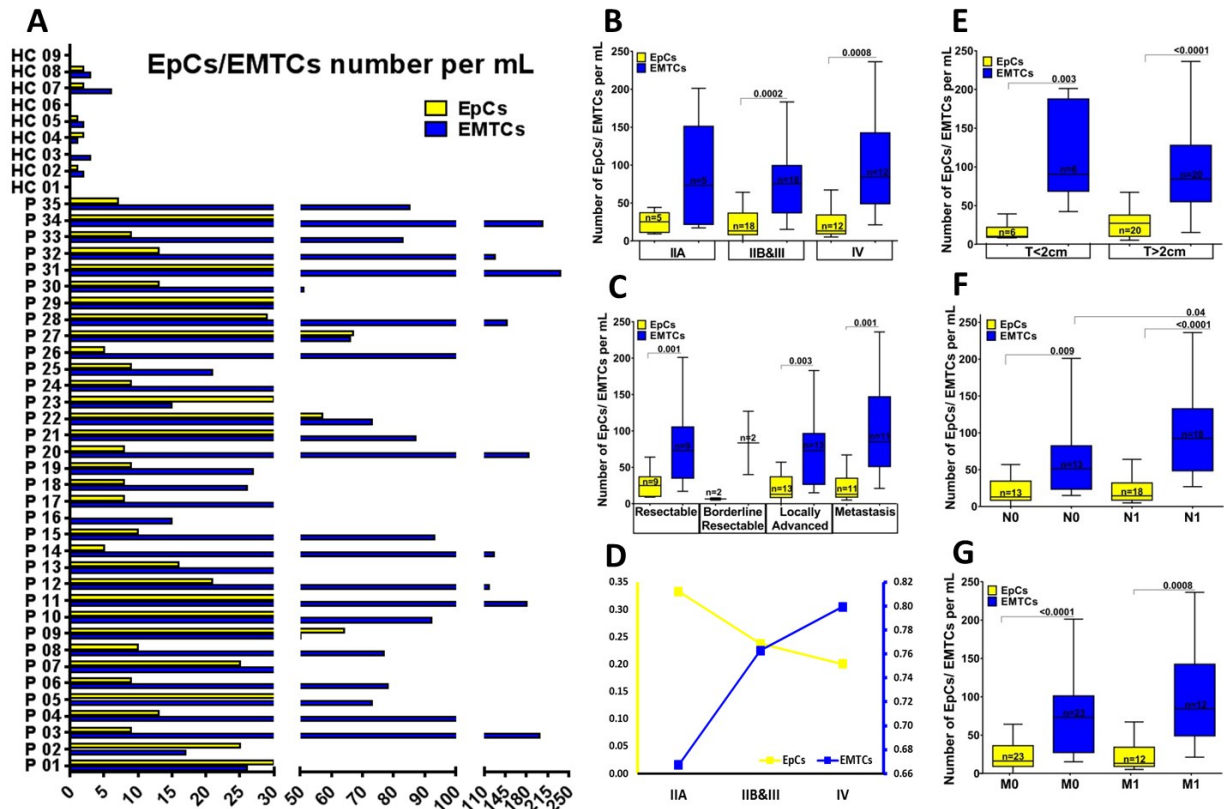
Figure 5: Analysis of EpCs and EMTCs from PaCa patient samples. A Enumeration of EpCs and EMTCs on the anti-EpCAM and anti-CD133 coated CTC Carpet Chips from PaCa patients (n=35) along with healthy controls (HCs) (n=9). Significant difference between the overall number of CTCs in PaCa patients samples (108.1±63.5) vs. HCs (2.8±2.6) (p<0.0001) was observed using unpaired t-tests (two-tailed). Significantly higher numbers of EMTCs (85.7±59.5) compared to EpCs (22.4±17.7) were observed (p<0.0001) using paired t-tests (two-tailed) (n=35). **B,C** Analysis of number of EpCs and EMTCs recovered in PaCa patient samples (n=35) based on their clinical disease stages from stage IIA (n=6), IIB&III (n=17), and IV (n=12), and based on tumor status (resectable (n=9), borderline resectabale (n=2), locally advanced (n=13) and metastatic (n=11)). No significant differences were observed in the effect of stage and resection on the number of EpCs and EMTCs using unpaired t-tests. **D** Ratio of EpCs to total number of CTCs and ratio of EMTCs to total number of CTCs from early to advanced stage disease. **E-G** Enumerated EpCs and EMTCs grouped according to tumor size (> or <2cm (E), lymph node involvement (N0 or N1) (F), and metastasis (M0 or M1) (G). Unpaired t-tests were used to analyze the effect of tumor size, lymph node involvement, and metastasis. N1 group (n=18) showed significantly higher number of EMTCs compared to N0 group (n=13) **(**p=0.04). No significant correlation between tumor size and metastatic burden were observed.
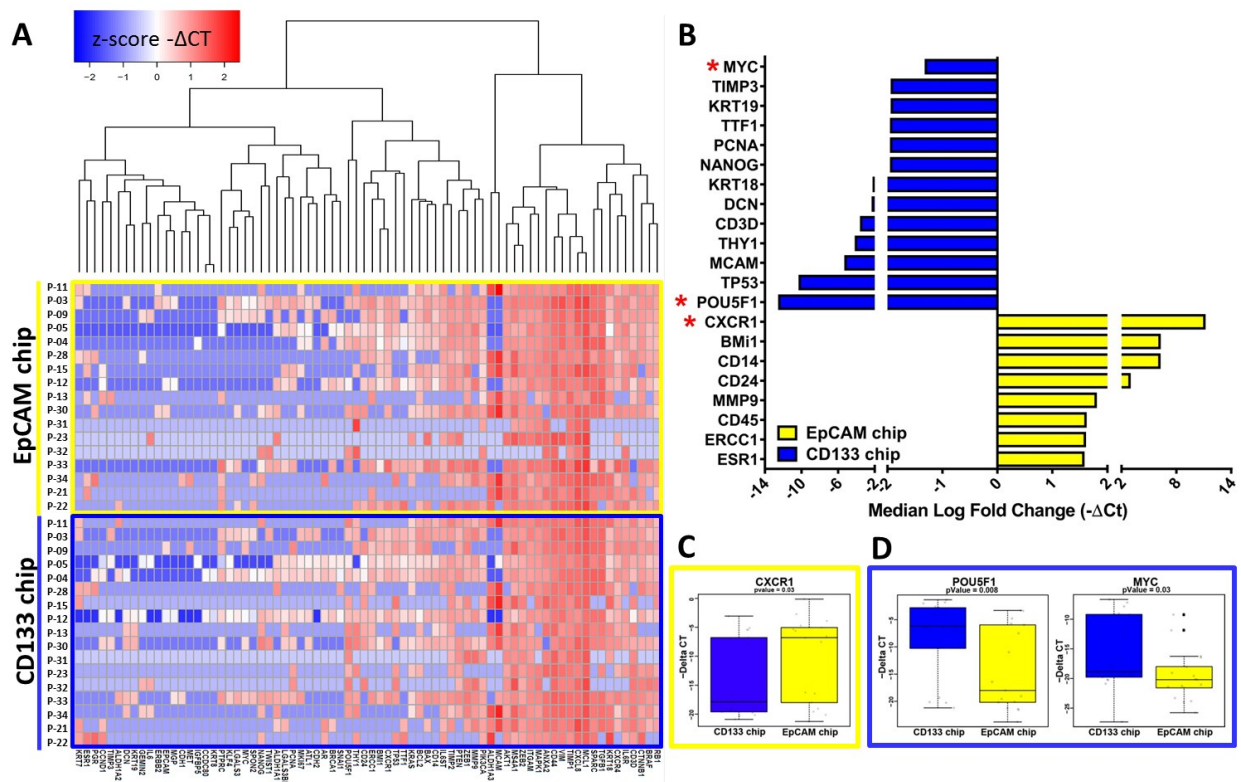
Figure 6: Gene expression profiling in PaCa patients CTC samples (n=17) based on capture device. A Clustering heat map analysis of gene expression data based on CTCs captured by EpCAM vs. CD133 CTC Carpet Chips was performed using -ΔCt. The top section shows the heat map of CTCs captured on EpCAM chip and the bottom section of the panel presents the CTCs captured on the CD133 chip. The color scale shown at the top illustrates the relative expression level of genes across the samples: red represents an expression level above the mean, blue represents expression lower than the mean. **B** The median log fold change (logFC) of selected genes with logFC>1.5 is shown in yellow (for the EpCAM chip) and blue (for the CD133 chip). Each fold change is calculated from the $2^{-\Delta Ct}$. **C,D** Box plot diagrams of significantly differently expressed individual genes in EpCAM chip, CXCR1 (p=0.03) and POU5F1 or Oct4 (p=0.008) and MYC (p=0.03) in CD133 chip. Yellow and blue bars represent the EpCAM and CD133 chips respectively. The Wilcoxon signed-rank test was used in RNA expression for paired samples (n=17).
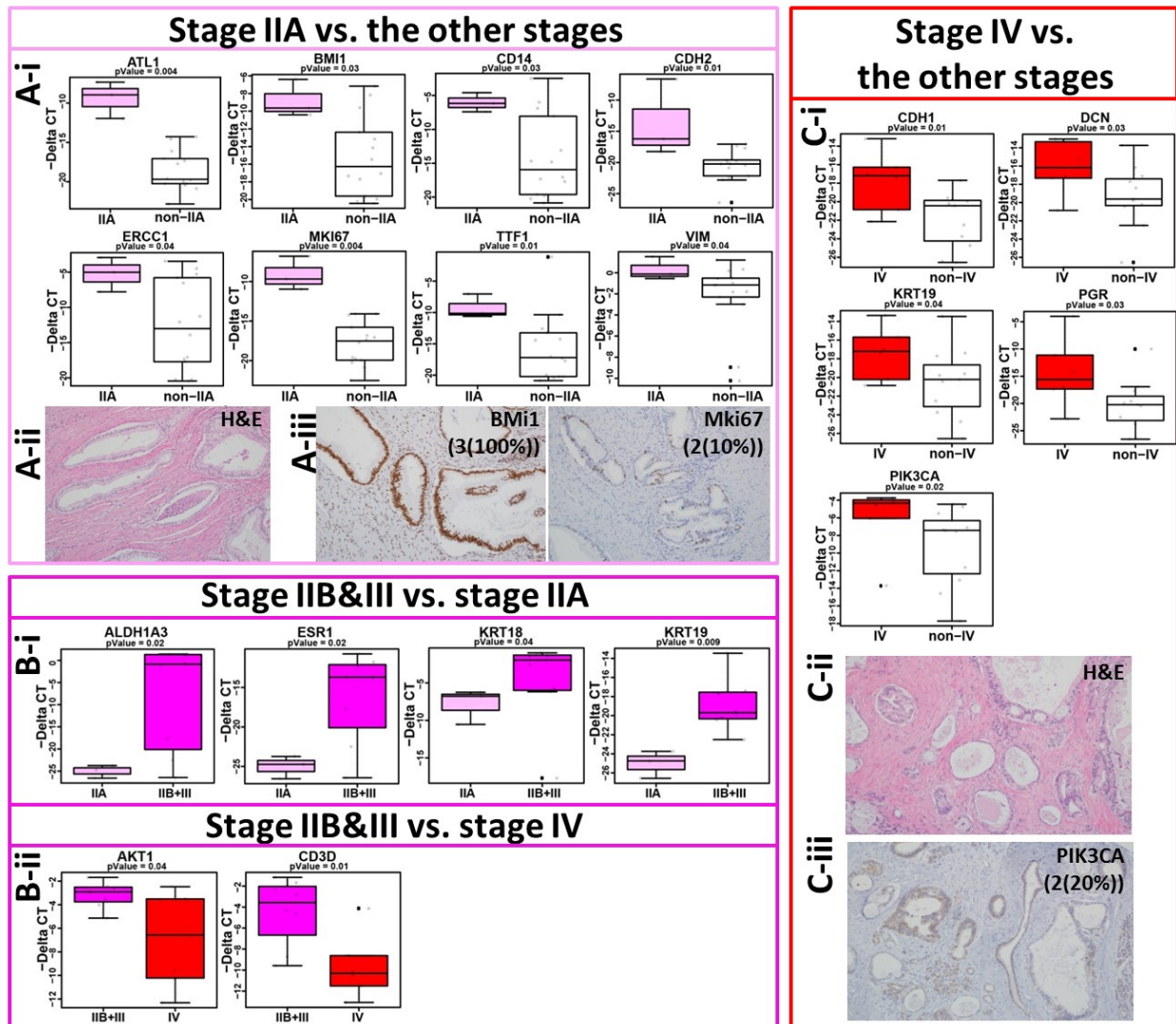
Figure 7: Gene expression profiling of CTCs based on PaCa patients categorized by disease stage. **A** Stage IIA samples (n=5) compared to the rest of stages (n=30) analysis**.** (A-i) Box plot diagrams of significantly (p<0.05) highly expressed individual genes in stage IIA CTC samples compared to the rest of stages including ATL1, BMi1, CD14, CDH2, ERCC1, MKi67, TTF1, and VIM genes, (A-ii) the H&E staining image of the primary tumor tissues of early stage patient, (A-iii) immunohistochemistry (IHC) analysis of the corresponding primary tumor tissues of early stage patients for BMi1 and MKi67 protein expressions revealed diffuse and strong positivity for BMi1 (intensity of 3 in 100% tumor cells), and patchy moderate positivity for Mki67 (intensity of 2 in 10%tumor cells) protein expression. **B** Box plot diagrams of significantly highly expressed individual genes in stage IIB&III CTC samples (n=18) compared with the early stage (n=5) including ALDH1A3, ESR1, KRT18 and 19 (B-i), and AKT1 and CD3D genes when stage IIB&III (n=18) compared with the late stage (n=12) (B-ii). **C** Stage IV CTC samples (n=12) compared to the rest of the stages (n=23) showed significantly over expression of genes including, CDH1, DCN, KRT19, PGR, and PIK3CA (C-i). The H&E staining image the primary tumor tissues of late stage patient (C-ii). PIK3CA protein expressions revealed patchy moderate positivity for this gene (intensity of 2 in 20%tumor cells) protein expression with IHC of primary tumor tissues (C-iii). (Original magnification: x100). The Mann-Whitney test was used to quantify differences in RNA expression for non-paired samples using the average -ΔCt value across both sample chips (n=17).
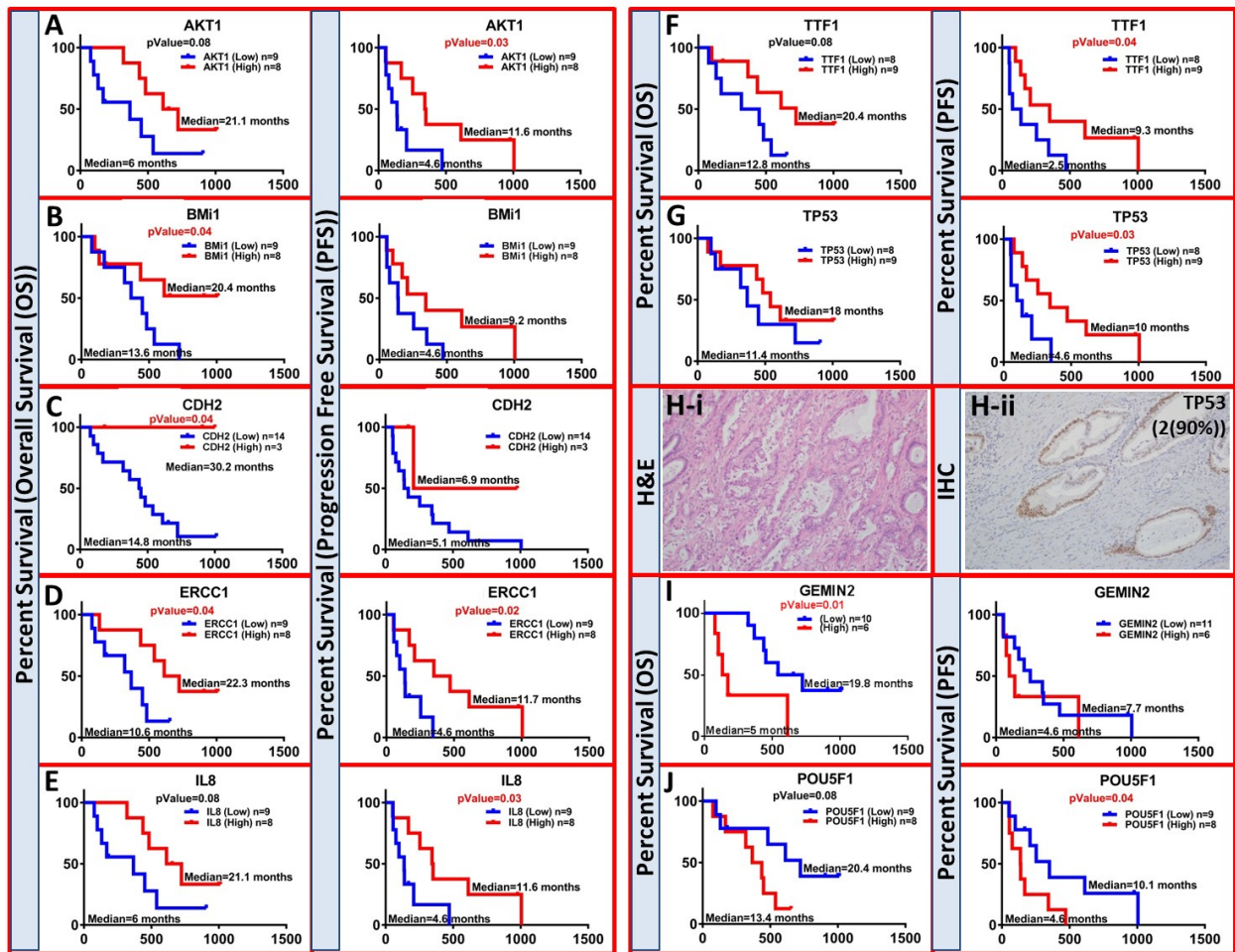
Figure 8: Relationship between CTCs gene expression and prognosis Comparison of Kaplan-Meier overall survival (OS) and progression free survival (PFS) graphs in all patient CTCs samples (n=17) with low (blue) and high (red) expressions of selected genes are shown. The median expression of each genes ($2^{-\Delta Ct}$) across all patients were used as cutoff points. Log-rank (Mantel-Cox) tests were used to analyze the Kaplan-Meier OS and PFS. **A-G** Higher expression of genes including BMi1, CDH2, and ERCC1 in PaCa patients showed significantly greater OS (p=0.04). Higher expression of genes including AKT1 (p=0.03), ERCC1 (p=0.02), IL8 (p=0.03), TTF1 (p=0.04), and TP53 (p=0.03) were significantly correlated with prolonged PFS. **H** The H&E staining image of (i) the primary tumor tissue, (ii) and TP53 marker showed diffuse positivity (intensity of 2 in 90% of tumor cells) of this marker in the corresponding primary tumor tissues. **I-J** Patients with high expression of genes including, GEMIN2 (p=0.01) and POU5F1 (p=0.04) had a worse OS and PFS respectively compared with those with low expression of these genes. (Original magnification: x100).